

Electrical Control of Skyrmion Density via Skyrmion-Stripe Transformation

Calvin Ching Ian Ang[✉], Weiliang Gan[✉], Grayson Dao Hwee Wong[✉], and Wen Siang Lew^{✉*}

School of Physical and Mathematical Sciences, Nanyang Technological University, 21 Nanyang Link, Singapore 637371, Singapore



(Received 17 August 2020; revised 3 October 2020; accepted 23 October 2020; published 19 November 2020)

A comprehensive understanding of numerous electrical current-induced magnetic texture transformations is necessary to ensure the reliability of skyrmionic devices during operation. Here, we present an experimental study of unipolar current-induced skyrmion-stripe transformation in a Pt/Co/Fe/Ir magnetic bilayer. High current density pulses induce a densely packed skyrmion state, as commonly reported in many other studies, and skyrmion nucleation is expected to lessen with diminishing current density. However, at a lower current density where pinning effects become significant, a regime where current-induced skyrmion annihilation and skyrmion-to-stripe transformation is observed. Kerr imaging reveals that, under a low current pulse, the rapidly expanding stripes crowd out and annihilate the skyrmions before quickly decaying and leaving behind a sparse skyrmion population. Our findings establish an additional requirement of a minimum operating current density in the design of skyrmionic devices to avoid unintended skyrmion deletion. On the other hand, this skyrmion annihilation can also be strategically employed as a technique for skyrmion density control using solely current modulation in future skyrmionic devices.

DOI: 10.1103/PhysRevApplied.14.054048

I. INTRODUCTION

Magnetic skyrmions are topologically stable magnetization states that are particlelike and nanoscale in size [1–4]. These magnetic skyrmions can be propagated using various techniques, such as spin torques [5–9], spin waves [10–12], electric fields [13], and magnetostatic energy gradients [14–19]. Hence, magnetic skyrmions are a promising candidate for nanoscale devices with a wide range of applications, such as memory storage [1], computational logic [20–23], neuromorphic computing [24–28], and probabilistic computing [29,30].

Among the different types of materials able to host magnetic skyrmions, sputtered magnetic multilayers with heavy metal/ferromagnetic interfaces, such as Pt/Co/Fe/Ir, are particularly advantageous. This structure provides a strong interfacial Dzyaloshinskii-Moriya interaction to stabilize magnetic skyrmions and ensure their homochirality [31–35]. Furthermore, the heavy metal layer's strong spin-orbit coupling supports a current-induced spin-orbit torque (SOT), which is efficient in driving skyrmions [5,6,36,37]. On top of that, their complementary metal-oxide-semiconductor (CMOS) compatibility allows electrical current-driven motion to be the preferred propagation technique for magnetic skyrmions.

In addition to propagation, electrical current pulses can be used for skyrmion nucleation [5,38–41], annihilation [41], and magnetic texture transformations [40,42,43].

Hence, a comprehensive understanding of all forms of electrical excitations is necessary for reliable performance. The stripe-to-skyrmion transformation has been reported in previous work as a skyrmion nucleation technique [5,38–40], where stripe domains were initially nucleated via magnetic field sweeps and subsequently broken into skyrmions by current pulses. In articles reporting the current-induced formation of stripes, these stripes were not shown to be created from skyrmions [42] or investigated at a magnetic field where these stripes showed decay into skyrmions thereafter [40,43]. In recent work, current-induced skyrmion-to-stripe transformation was reported but the underlying mechanism remains unclear [44].

In this work, we observe the current density dependence of the current-induced magnetization state transformation. A high current density induces the nucleation of skyrmions, whereas a low current density induces skyrmion-to-stripe transformation and skyrmion annihilation. The conditions required for the low current-induced transformation are determined to be millisecond pulses and an out-of-plane magnetic field with the skyrmion ground state. By utilizing the observed phenomena, the electrical control of skyrmion density is demonstrated using unipolar current pulses to activate the different current-induced magnetization states.

II. EXPERIMENTAL METHODS

A Ta(5)/Ir(2)/[Pt(1)/Co(0.5)/Fe(0.5)/Ir(0.8)]₂/Ta(5) (nominal layer thicknesses in nanometers) stack is grown

* wensiang@ntu.edu.sg

on a thermally oxidized silicon wafer by a magnetron sputtering system (AJA ATC-Orion 8) at room temperature. The base pressure of the vacuum chamber is better than 8×10^{-8} Torr, and a range of sputtering pressures of 2.0–3.0 mTorr is used during the film deposition. The bottom Ta(5) layer is used as an adhesive underlayer while the additional Ir(2) underlayer is added to provide a similar interface for the repeating layers. The top Ta(5) layer is used as a protective layer against oxidation. The film stack is patterned into a $20 \mu\text{m} \times 10 \mu\text{m}$ Hall cross structure using a combination of electron beam lithography and ion milling techniques.

Images of magnetic domains are captured using a MagVision Kerr Imaging System, which operates on the magneto-optical Kerr effect (MOKE) in the polar configuration. In the polar configuration, the out-of-plane magnetization is probed and observed as different levels of brightness in the image. In the images, regions of lower brightness correspond to magnetization in the negative out-of-plane direction and vice versa. The images' color balance is adjusted to offer the best contrast for qualitative analysis.

Four-point configuration is used to measure Hall resistance using a Keithley 2401 sourcemeter. A measuring current is passed across the wider bar while the Hall resistance measurement is performed across the narrow bar. The measuring current has a current density of $1.38 \times 10^9 \text{ A/m}^2$ and a duration of 85 ms.

III. RESULTS AND DISCUSSION

A. Current-induced skyrmion-stripe transformation

The optical micrograph of the patterned Hall cross structure is shown in Fig. 1(a). An out-of-plane magnetic field H_Z of 18.8 Oe is applied to initialize a magnetic state with only skyrmions. Upon applying a magnetic field, the magnetization evolves gradually towards the equilibrium state. The sample is left idle for 3 min to reach its equilibrium state. For each current density investigated between the range of $1.11 \times 10^{10} \text{ A/m}^2$ to $7.75 \times 10^{10} \text{ A/m}^2$, 30 pulses of 10 ms duration are injected across the wide bar as indicated in Fig. 1(a). The subsequent relaxation process after these pulse injections is given by the Hall resistance R_{Hall} . Here, a positive ΔR_{Hall} corresponds to an increase in net magnetization in the direction of H_Z , which also implies the annihilation of stripes or skyrmions and vice versa.

The difference in current-induced magnetization states is deduced based on the ΔR_{Hall} trend during the relaxation process. From Fig. 1(b), the low current density pulses induce the relaxation process with an initial ΔR_{Hall} , which increases up to a peak before decaying into the final equilibrium state. The highest ΔR_{Hall} peak is observed at the current density of $2.21 \times 10^{10} \text{ A/m}^2$. As current density is increased to $3.32 \times 10^{10} \text{ A/m}^2$, the ΔR_{Hall} peak decreases in magnitude and eventually vanishes at $3.88 \times 10^{10} \text{ A/m}^2$.

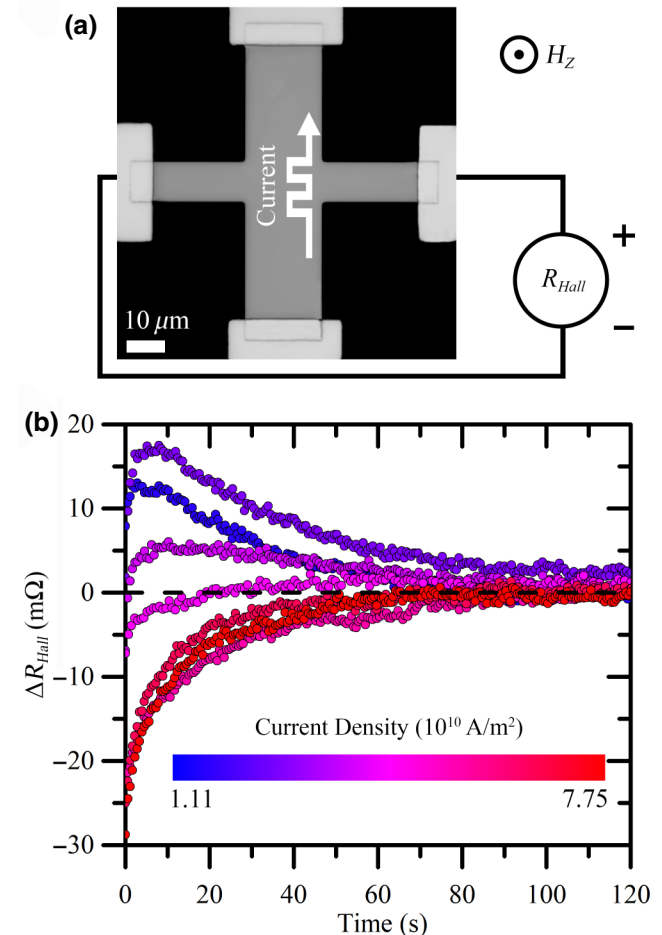


FIG. 1. Hall resistance measurement of the relaxation process of current-induced magnetization transformation. (a) Measurement setup consisting of a Hall cross with widths of 20 and $10 \mu\text{m}$. Electrical currents are injected through the wider Hall bar while Hall resistance R_{Hall} is measured across the narrow bar. (b) Time evolution of Hall resistance change ΔR_{Hall} after 30 current pulses of 10 ms are injected for current densities ranging from $1.11 \times 10^{10} \text{ A/m}^2$ to $7.75 \times 10^{10} \text{ A/m}^2$. Error bars are omitted from the graph for clarity, and the data have a standard deviation of $6 \text{ m}\Omega$ or less.

At current densities higher than $3.88 \times 10^{10} \text{ A/m}^2$, the initial ΔR_{Hall} is lower than equilibrium and increases at a decreasing rate towards the equilibrium state. Lastly, for current densities above $5.54 \times 10^{10} \text{ A/m}^2$, ΔR_{Hall} trends remain almost unchanged suggesting that the current-induced magnetization states and their relaxation process reach a limiting condition.

To observe the different current-induced magnetization states and their relaxation process dependence on electrical current density, MOKE imaging is performed. Figure 2(a) shows the equilibrium state of the wire where the wire is densely packed with magnetic skyrmions. Figures 2(b)–2(d) show the MOKE images taken at 0.4 s, 12.1 s, and 41.4 s, respectively, after injecting current pulses of

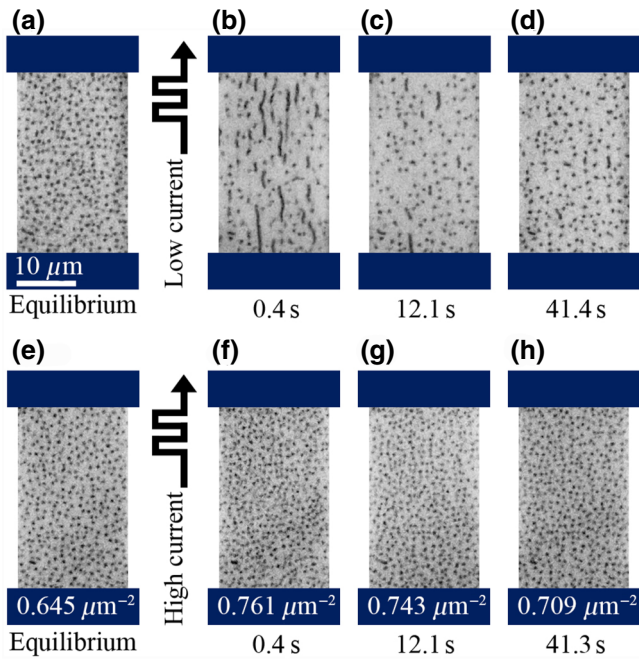


FIG. 2. MOKE images of current-induced magnetic states and their relaxation process back to equilibrium. (a) Magnetization state at equilibrium. After the injection of $2.21 \times 10^{10} \text{ A/m}^2$ current pulses, the skyrmions are transformed into a mixed state of stripes and skyrmions at (b) $t = 0.4 \text{ s}$. Magnetization state at (c) $t = 12.1 \text{ s}$ and (d) $t = 41.4 \text{ s}$ after current injection. (e) Magnetization state at equilibrium with skyrmion density of $0.645 \mu\text{m}^{-2}$. After the injection of $7.20 \times 10^{10} \text{ A/m}^2$ current pulses, a state with a higher skyrmion density of $0.761 \mu\text{m}^{-2}$ is observed at (f) $t = 0.4 \text{ s}$. The high skyrmion density state shows a gradual reduction in density at (g) $t = 12.1 \text{ s}$ and (h) $t = 41.3 \text{ s}$, with skyrmion density of $0.743 \mu\text{m}^{-2}$, and $0.709 \mu\text{m}^{-2}$, respectively. The states in (d) and (h) eventually return to the equilibrium state.

$2.21 \times 10^{10} \text{ A/m}^2$. After the pulses are injected, the magnetization state transforms into one with sparse skyrmion density along with newly formed stripes. The formation of stripes crowds out the skyrmions and causes part of the skyrmion population to be annihilated into the ferromagnetic state. These stripes gradually shrink into skyrmions, leaving behind regions in the ferromagnetic state. With time, the spontaneous nucleation of skyrmions gradually fills the wire as shown in Fig. 2(d), and the wire returns to the equilibrium state. The peaking of ΔR_{Hall} observed in Fig. 1(b) can then be attributed to the two competing processes: the shrinking of stripes into skyrmions, which increases Hall resistance, and the spontaneous nucleation of skyrmions, which decreases Hall resistance.

In contrast to the observation for current pulses with the lower current density of $2.21 \times 10^{10} \text{ A/m}^2$, the higher current density pulses of $7.20 \times 10^{10} \text{ A/m}^2$ induce a proliferation of skyrmions that increase the skyrmion density from $0.645 \mu\text{m}^{-2}$ to $0.761 \mu\text{m}^{-2}$ as shown in Figs. 2(e) and 2(f). The skyrmion density gradually reduces to

$0.743 \mu\text{m}^{-2}$ and $0.709 \mu\text{m}^{-2}$ as shown in Figs. 2(g) and 2(h). This transformation is visually subtle but remains in agreement with the ΔR_{Hall} results shown in Fig. 1(b), where the current injection induces a negative ΔR_{Hall} , corresponding to the nucleation of skyrmions. While a larger current can be expected to nucleate more skyrmions, a limiting condition exists as the skyrmion density is limited by skyrmion-skyrmion repulsion [45,46]. Even though the skyrmion density can be raised above this limit, it is not a stable state and excess skyrmions will annihilate until the equilibrium skyrmion density is reached.

The long timescale of magnetic state transition observed in this work is primarily due to the thermally activated transitions between the ferromagnetic state and skyrmion state. The creeping motion of stripe domains as they shrink back into skyrmions is also in the timescale of seconds, but ultimately the transition time is dominated by the even slower spontaneous nucleation and annihilation of skyrmions.

B. Current pulse duration

The wire is initialized following the same procedure as in Sec. III A; an out-of-plane magnetic field of 18.8 Oe is applied and left idle for 3 min. However, only a single current pulse is used in this section. While the negative ΔR_{Hall} induced by higher current densities remains observable for pulse durations as short as $10 \mu\text{s}$, the ΔR_{Hall} peak associated with lower current densities becomes barely observable for a pulse duration of 1 ms or less. Based on the mechanism of the magnetic texture transformations due to low current excitation revealed in the previous section, the relative value of the ΔR_{Hall} peak correlates to the number of stripe domains formed and the general effectiveness of the low current pulse in decreasing skyrmion density. The peak value of ΔR_{Hall} increases with pulse duration as shown in the inset of Fig. 3(a). Figure 3(a) shows that the maximum ΔR_{Hall} quickly approaches a saturation value with pulse durations above 10 ms. Comparing Figs. 3(b) and 3(c) the increasing Hall resistance peak corresponds to the lower minimum skyrmion density reached during the relaxation process caused by the increased number of stripes formed. Figure 3(d) shows that the stripe formation does not increase indefinitely and approaches a limiting number of stripes.

In investigating the skyrmion-to-stripe transformation mechanism, it is observed that the stripes tend to form from several spots on the wire after low current injection. In addition, stripes of differing lengths in the direction of the current consistently formed from these same spots, which correspond to pinning sites. It is therefore likely that the stripes are nucleated due to skyrmion-pinning site interactions, where a skyrmion is pinned at a defect and becomes elongated due to the propagative force caused by the injected current pulse. Similar elongation phenomena have

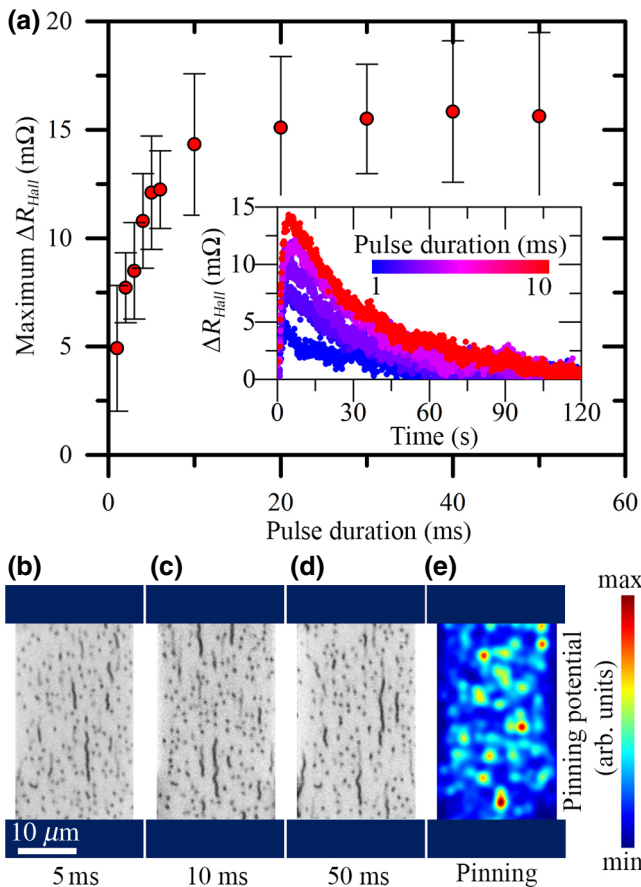


FIG. 3. Current-induced stripe formation dependence on pulse duration. (a) The plot of maximum ΔR_{Hall} during the relaxation process after low current pulse injection against pulse duration. The inset provides the plot of Hall resistance change ΔR_{Hall} over time for pulse durations ranging from 1 to 10 ms. Error bars correspond to the standard deviation. MOKE images are taken immediately after current pulse injections with a pulse duration of (b) 5 ms, (c) 10 ms, and (d) 50 ms. (e) Relative pinning potential along the wire obtained from 100 images of skyrmion-to-stripe transformation.

been reported recently, where stripes extended from the edges of existing domains after current injections [47,48]. The pinning potential map of the wire shown in Fig. 3(e) is generated using images from 100 iterations of stripe formation cycles. In each iteration, the wire is first left idle to reach equilibrium, then injected with a single low-current pulse, and imaged once immediately afterwards. The pinned ends of the stripe domains formed are identified in each image and summed across all iterations to generate an overall spatial pinning potential across the wire.

C. Out-of-plane magnetic field

The observations for the low current density transformation presented thus far have been performed at

H_Z of 18.8 Oe, a field close to the saturation field where the ground state is characterized by densely packed skyrmions. The current-induced transformations are also investigated for the full range of H_Z below saturation where the ground state ranges from labyrinth domains to stripes and skyrmions. The investigation is executed similarly using 30 pulses of 10 ms at a current density of $2.21 \times 10^{10} \text{ A/m}^2$.

In the absence of an external magnetic field, the ground state of the wire is the labyrinth configuration. Current injection transforms the initial labyrinth domain into parallel stripes aligned in the direction of the current as shown in Fig. 4(a). Increasing H_Z to 13.4 Oe, skyrmions with diameters of approximately 700 nm start to form while the labyrinth domains break into stripes. In this range of H_Z , the current-induced magnetization states start to form shorter stripes that remain aligned in the direction of current as shown in Figs. 4(b) and 4(c). The current-induced magnetization states formed in the range of 0.0 to 10.1 Oe are stable and do not show significant changes in domain texture over time.

For the H_Z range of 13.4 to 20.1 Oe, the current-induced formation of stripe domains is observed as shown in Figs. 4(d) and 4(e). These then shrink over time into skyrmions following the same process previously given in Fig. 2. By comparing Figs. 4(d) and 4(e) it can be seen that the current forms fewer and shorter stripes with increasing H_Z . The skyrmion diameter also shrinks down to approximately 500 nm. At the saturation field of 23.5 Oe, the current-induced phenomenon is no longer observed due to the large Zeeman energy that restricts any transformation into other magnetic configurations.

In Fig. 4(f), the current-induced phenomena are analyzed quantitatively by the comparison of the maximum ΔR_{Hall} achieved during relaxation at each magnetic field. A clear peak is found at approximately 20 Oe. A common trend is seen between the current-induced state ΔR_{Hall} and maximum ΔR_{Hall} within the H_Z range of 16.8 to 23.5 Oe. This range of H_Z also closely coincides with the diverging segment of the magnetic hysteresis where irreversible magnetization transformations take place.

D. Skyrmion density control

The contrasting magnetization states induced by high and low current density injection presents an opportunity for applications in skyrmion density control using a unipolar current. A series of current pulses alternating between low ($2.21 \times 10^{10} \text{ A/m}^2$) and high ($5.54 \times 10^{10} \text{ A/m}^2$) current density is injected as shown in Fig. 5. The magnetization state can be interchangeably transformed between the low and high skyrmion density state by injecting low and high current density currents, respectively. Although these states eventually return to the equilibrium state, this technique remains applicable to skyrmions with higher

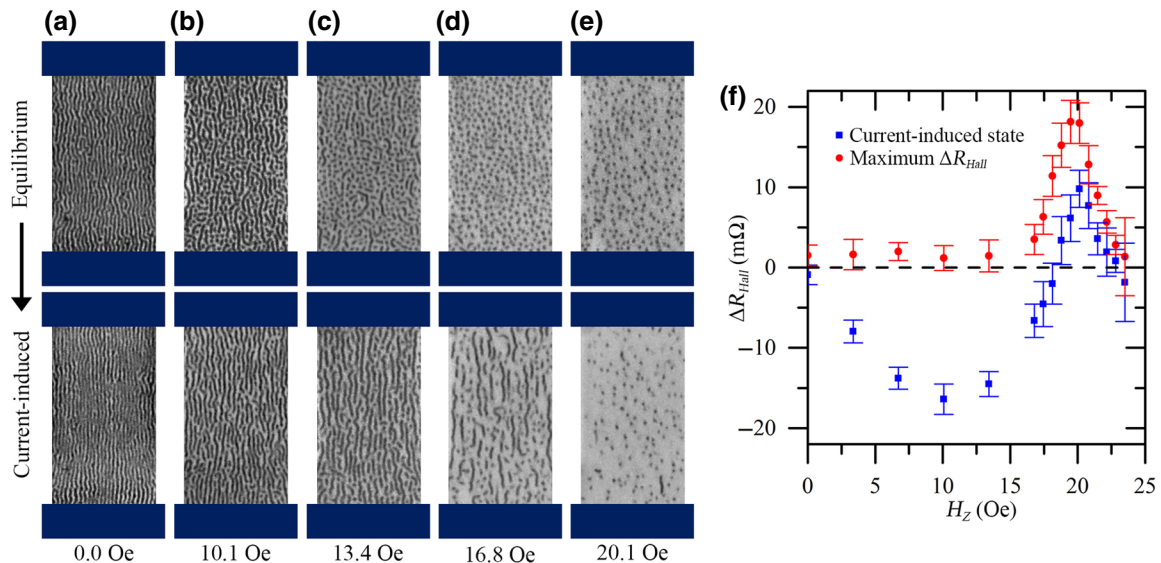


FIG. 4. Current-induced magnetization state dependence on the out-of-plane magnetic field. MOKE images of their equilibrium and current-induced magnetization state at H_Z of (a) 0.0 Oe, (b) 10.1 Oe, (c) 13.4 Oe, (d) 16.8 Oe, and (e) 20.1 Oe. (f) The plot of the initial current-induced state's ΔR_{Hall} and its corresponding maximum ΔR_{Hall} during relaxation against H_Z . Error bars correspond to the standard deviation.

thermal stability and can be used to produce nonvolatile state transformations.

E. Discussion

Based on the evidence presented previously, the skyrmion-to-stripe transformation is found to occur under the conditions of (i) an out-of-plane magnetic field where stripes are unstable and only skyrmions are stabilized, (ii) a long pulse duration of the order of milliseconds, and (iii) a low current magnitude range of 1.11×10^{10} to 3.32×10^{10} A/m². By utilizing this phenomenon, one

can achieve two-way skyrmion density modulation under a constant magnetic field.

In materials with Pt/Co, pinning sites are expected due to the sputtering process, its polycrystalline structure, and grain boundaries. As current density increases, the skyrmions are less likely to be pinned, which explains the lack of stripe nucleation at high current density. Higher current density injection, on the other hand, induces nucleation of skyrmions with a higher density than that of the equilibrium state.

Joule heating has been closely associated with magnetic texture transformations and skyrmion nucleation in the literature [39–41,49,50], but is found to be negligible and not the main contributor to the current-induced skyrmion-to-stripe transformation or current-induced skyrmion annihilation in this work (see Supplemental Material [52]). The current pulses used in the study are found to produce no measurable increase in temperature. However, by applying a longer pulse of 352 ms, we can establish an upper bound of 1 K change in temperature. Hence, the current-induced phenomena observed in this work is not likely to be due to Joule heating.

While the skyrmion-to-stripe transformation is dependent on the current pulse duration of the order of milliseconds, it is due to the slow elongation of the domain in the creep regime. The nucleation mechanism of skyrmions under high current density can be attributed to SOT induced nucleation in nonuniform pinning potential [43,51]. The presence of a SOT in our multilayer is evident from the current-driven motion of magnetic skyrmions along the direction of current as shown in the video in the Supplemental Material [52]. Hence, pinning

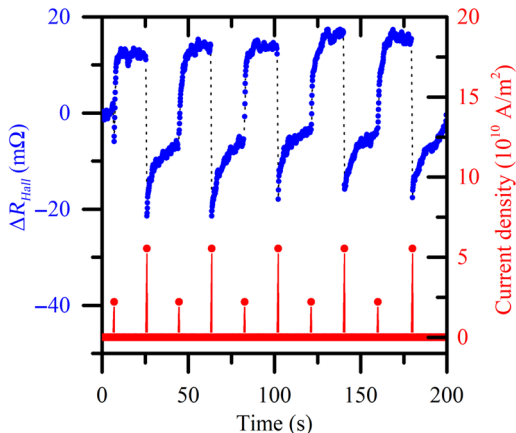


FIG. 5. Demonstration of electrical control of skyrmion density. The plot of ΔR_{Hall} as a measure of skyrmion density over time due to alternating pulses of low (2.21×10^{10} A/m²) and high (5.51×10^{10} A/m²) current densities.

potential is the key property that allows for skyrmion nucleation, skyrmion annihilation, and skyrmion-to-stripe transformation.

The timescale of magnetic texture transformation shown in Fig. 1(b) is intentionally adjusted to the order of seconds and tens of seconds by adjusting the out-of-plane magnetic field to acquire MOKE images, which requires seconds of exposure time. With higher out-of-plane magnetic fields, stripe domains become less favorable as shown in Figs. 4(a)–4(e), and the timescale of the transformation decreases. With tuning of the operating out-of-plane magnetic field, and fabricating artificial pinning sites, the volatile nature of the stripes formed from skyrmion-to-stripe transformation at a pinning site can be applied in neuromorphic devices. For instance, the mimicking of a leaky-integrate fire neuron requires the property of potential decay over time after excitation, and artificial synapses with short-term plasticity where their states are only temporarily retained. Nonetheless, the primary phenomena raised in the manuscript, skyrmion-to-stripe transformation due to pinning, remains a valuable consideration for the design of future skyrmionic devices.

IV. CONCLUSIONS

In conclusion, we report the observation of current-induced skyrmion annihilation and skyrmion-stripe transformation at low current density due to pinning effects. By utilizing this phenomenon together with the nucleation of skyrmions at high current density, its application as a technique for skyrmion density control that only requires the use of a unipolar electrical current is demonstrated. The current-induced skyrmion annihilation reported here also has implications on the operating current densities of future skyrmionic devices where pinning effects are significant. Our study further advances the understanding of current-induced phenomena on magnetic skyrmions for the development of future skyrmionic devices.

ACKNOWLEDGMENTS

This work is supported by the Singapore National Research Foundation, Prime Minister's Office under a Competitive Research Programme (Non-volatile Magnetic Logic and Memory Integrated Circuit Devices, NRF-CRP9-2011-01), and an Industry-IHL Partnership Program (NRF2015-IIP001-001). The support from a RIE2020 ASTAR AME IAF-ICP Grant (No.I1801E0030) is also acknowledged. W.S.L. is a member of the SG-SPIN Consortium.

[1] A. Fert, V. Cros, and J. Sampaio, Skyrmions on the track, *Nat. Nanotech.* **8**, 152 (2013).

- [2] N. Nagaosa and Y. Tokura, Topological properties and dynamics of magnetic skyrmions, *Nat. Nanotech.* **8**, 899 (2013).
- [3] R. Wiesendanger, Nanoscale magnetic skyrmions in metallic films and multilayers: A new twist for spintronics, *Nat. Rev. Mater.* **1**, 16044 (2016).
- [4] A. Fert, N. Reyren, and V. Cros, Magnetic skyrmions: Advances in physics and potential applications, *Nat. Rev. Mater.* **2**, 17031 (2017).
- [5] W. Jiang, P. Upadhyaya, W. Zhang, G. Yu, M. B. Jungfleisch, F. Y. Fradin, J. E. Pearson, Y. Tserkovnyak, K. L. Wang, O. Heinonen, S. G. E. te Velthuis, and A. Hoffmann, Blowing magnetic skyrmion bubbles, *Science* **349**, 283 (2015).
- [6] S. Woo, K. Litzius, B. Krüger, M.-Y. Im, L. Caretta, K. Richter, M. Mann, A. Krone, R. M. Reeve, M. Weigand, P. Agrawal, I. Lemesh, M.-A. Mawass, P. Fischer, M. Kläui, and G. S. D. Beach, Observation of room-temperature magnetic skyrmions and their current-driven dynamics in ultrathin metallic ferromagnets, *Nat. Mater.* **15**, 501 (2016).
- [7] W. Jiang, X. Zhang, G. Yu, W. Zhang, X. Wang, M. Benjamin Jungfleisch, John E. Pearson, X. Cheng, O. Heinonen, K. L. Wang, Y. Zhou, A. Hoffmann, and Suzanne G. E. te Velthuis, Direct observation of the skyrmion hall effect, *Nat. Phys.* **13**, 162 (2016).
- [8] F. Luo, Q. Y. Wong, S. Li, F. Tan, G. J. Lim, X. Wang, and W. S. Lew, Dependence of spin-orbit torque effective fields on magnetization uniformity in Ta/Co/Pt structure, *Sci. Rep.* **9**, 10776 (2019).
- [9] T. Dohi, S. DuttaGupta, S. Fukami, and H. Ohno, Formation and current-induced motion of synthetic antiferromagnetic skyrmion bubbles, *Nat. Commun.* **10**, 5153 (2019).
- [10] C. Schütte and M. Garst, Magnon-skyrmion scattering in chiral magnets, *Phys. Rev. B* **90**, 094423 (2014).
- [11] J. Iwasaki, A. J. Beekman, and N. Nagaosa, Theory of magnon-skyrmion scattering in chiral magnets, *Phys. Rev. B* **89**, 064412 (2014).
- [12] X. Zhang, M. Ezawa, D. Xiao, G. P. Zhao, Y. Liu, and Y. Zhou, All-magnetic control of skyrmions in nanowires by a spin wave, *Nanotechnology* **26**, 225701 (2015).
- [13] C. Ma, X. Zhang, J. Xia, M. Ezawa, W. Jiang, T. Ono, S. N. Piramanayagam, A. Morisako, Y. Zhou, and X. Liu, Electric field-induced creation and directional motion of domain walls and skyrmion bubbles, *Nano Lett.* **19**, 353 (2019).
- [14] K. Everschor, M. Garst, B. Binz, F. Jonietz, S. Mühlbauer, C. Pfleiderer, and A. Rosch, Rotating skyrmion lattices by spin torques and field or temperature gradients, *Phys. Rev. B* **86**, 054432 (2012).
- [15] C. Wang, D. Xiao, X. Chen, Y. Zhou, and Y. Liu, Manipulating and trapping skyrmions by magnetic field gradients, *New J. Phys.* **19**, 083008 (2017).
- [16] X. Wang, W. L. Gan, J. C. Martinez, F. N. Tan, M. B. A. Jalil, and W. S. Lew, Efficient skyrmion transport mediated by a voltage controlled magnetic anisotropy gradient, *Nanoscale* **10**, 733 (2018).
- [17] F. N. Tan, W. L. Gan, C. C. I. Ang, G. D. H. Wong, H. X. Liu, F. Poh, and W. S. Lew, High velocity domain wall propagation using voltage controlled magnetic anisotropy, *Sci. Rep.* **9**, 7369 (2019).

- [18] C. C. I. Ang, W. Gan, and W. S. Lew, Bilayer skyrmion dynamics on a magnetic anisotropy gradient, *New J. Phys.* **21**, 043006 (2019).
- [19] Y. Liu, X. Huo, S. Xuan, and H. Yan, Manipulating movement of skyrmion by strain gradient in a nanotrack, *J. Magn. Magn. Mater.* **492**, 165659 (2019).
- [20] S. Luo, M. Song, X. Li, Y. Zhang, J. Hong, X. Yang, X. Zou, N. Xu, and L. You, Reconfigurable skyrmion logic gates, *Nano Lett.* **18**, 1180 (2018).
- [21] M. Chauwin, X. Hu, F. Garcia-Sanchez, N. Betrabet, A. Paler, C. Moutafis, and J. S. Friedman, Skyrmion Logic System for Large-Scale Reversible Computation, *Phys. Rev. Appl.* **12**, 064053 (2019).
- [22] M. G. Mankalale, Z. Zhao, J. Wang, and S. S. Saputnekar, Skylogic—A proposal for a skyrmion-based logic device, *IEEE Trans. Electron Devices* **66**, 1990 (2019).
- [23] S. Luo, M. Song, M. Shen, Y. Zhang, J. Hong, and L. You, Skyrmion latch and flip-flop in magnetic nanotacks with gradient anisotropy, *J. Magn. Magn. Mater.* **494**, 165739 (2020).
- [24] F. Garcia-Sanchez, J. Sampaio, N. Reyren, V. Cros, and J. V. Kim, A skyrmion-based spin-torque nano-oscillator, *New J. Phys.* **18**, 075011 (2016).
- [25] D. Fan, Z. He, and S. Angizi, in *2017 IEEE 60th International Midwest Symposium on Circuits and Systems (MWSCAS)Medford*, MA, United States, (2017), pp. 1109.
- [26] Z. He and D. Fan, in *Design, Automation & Test in Europe Conference & Exhibition (DATE)Lausanne*, Switzerland, (2017), pp. 350.
- [27] M. A. Azam, D. Bhattacharya, D. Querlioz, and J. Atulasimha, Resonate and fire neuron with fixed magnetic skyrmions, *J. Appl. Phys.* **124**, 152122 (2018).
- [28] X. Chen, W. Kang, D. Zhu, X. Zhang, N. Lei, Y. Zhang, Y. Zhou, and W. Zhao, A compact skyrmionic leaky-integrate-fire spiking neuron device, *Nanoscale* **10**, 6139 (2018).
- [29] D. Pinna, F. Abreu Araujo, J. V. Kim, V. Cros, D. Querlioz, P. Bessiere, J. Droulez, and J. Grollier, Skyrmion Gas Manipulation for Probabilistic Computing, *Phys. Rev. Appl.* **9**, 064018 (2018).
- [30] J. Zázvorka, F. Jakobs, D. Heinze, N. Keil, S. Kromin, S. Jaiswal, K. Litzius, G. Jakob, P. Virnau, D. Pinna, K. Everschor-Sitte, L. Rózsa, A. Donges, U. Nowak, and M. Kläui, Thermal skyrmion diffusion used in a reshuffler device, *Nat. Nanotechnol.* **14**, 658 (2019).
- [31] I. Dzyaloshinsky, A thermodynamic theory of “weak” ferromagnetism of antiferromagnetics, *J. Phys. Chem. Solids* **4**, 241 (1958).
- [32] T. Moriya, Anisotropic superexchange interaction and weak ferromagnetism, *Phys. Rev.* **120**, 91 (1960).
- [33] A. Crépieux and C. Lacroix, Dzyaloshinsky–moriya interactions induced by symmetry breaking at a surface, *J. Magn. Magn. Mater.* **182**, 341 (1998).
- [34] A. Fert and P. M. Levy, Role of Anisotropic Exchange Interactions in Determining the Properties of Spin-Glasses, *Phys. Rev. Lett.* **44**, 1538 (1980).
- [35] A. Soumyanarayanan, M. Raju, A. L. Gonzalez Oyarce, A. K. C. Tan, M.-Y. Im, A. P. Petrović, P. Ho, K. H. Khoo, M. Tran, C. K. Gan, F. Ernult, and C. Panagopoulos, Tunable room-temperature magnetic skyrmions in Ir/Fe/Co/Pt multilayers, *Nat. Mater.* **16**, 898 (2017).
- [36] S. Woo, K. M. Song, H.-S. Han, M.-S. Jung, M.-Y. Im, K.-S. Lee, K. S. Song, P. Fischer, J.-I. Hong, J. W. Choi, B.-C. Min, H. C. Koo, and J. Chang, Spin-orbit torque-driven skyrmion dynamics revealed by time-resolved X-ray microscopy, *Nat. Commun.* **8**, 15573 (2017).
- [37] S. A. Montoya, R. Tolley, I. Gilbert, S.-G. Je, M.-Y. Im, and E. E. Fullerton, Spin-orbit torque induced dipole skyrmion motion at room temperature, *Phys. Rev. B* **98**, 104432 (2018).
- [38] W. Jiang, W. Zhang, G. Yu, M. B. Jungfleisch, P. Upadhyaya, H. Somailey, J. E. Pearson, Y. Tserkovnyak, K. L. Wang, O. Heinonen, S. G. E. te Velthuis, and A. Hoffmann, Mobile Néel skyrmions at room temperature: Status and future, *AIP Adv.* **6**, 055602 (2016).
- [39] W. Legrand, D. Maccariello, N. Reyren, K. Garcia, C. Moutafis, C. Moreau-Luchaire, S. Collin, K. Bouzehouane, V. Cros, and A. Fert, Room-Temperature current-induced generation and motion of sub-100 nm skyrmions, *Nano Lett.* **17**, 2703 (2017).
- [40] I. Lemesh, K. Litzius, M. Böttcher, P. Bassirian, N. Kerber, D. Heinze, J. Zázvorka, F. Büttner, L. Caretta, M. Mann, M. Weigand, S. Finizio, J. Raabe, M.-Y. Im, H. Stoll, G. Schütz, B. Dupé, M. Kläui, and G. S. D. Beach, Current-Induced skyrmion generation through morphological thermal transitions in chiral ferromagnetic heterostructures, *Adv. Mater.* **30**, 1805461 (2018).
- [41] S.-G. Je, M.-S. Jung, M.-Y. Im, and J.-I. Hong, Electric current control of creation and annihilation of sub-100 nm magnetic bubbles examined by full-field transmission soft X-ray microscopy, *Curr. Appl. Phys.* **18**, 1201 (2018).
- [42] G. Yu, P. Upadhyaya, Q. Shao, H. Wu, G. Yin, X. Li, C. He, W. Jiang, X. Han, P. K. Amiri, and K. L. Wang, Room-Temperature skyrmion shift device for memory application, *Nano Lett.* **17**, 261 (2017).
- [43] F. Büttner, I. Lemesh, M. Schneider, B. Pfau, C. M. Günther, P. Hessing, J. Geihufe, L. Caretta, D. Engel, B. Krüger, J. Viehaus, S. Eisebitt, and G. S. D. Beach, Field-free deterministic ultrafast creation of magnetic skyrmions by spin-orbit torques, *Nat. Nanotechnol.* **12**, 1040 (2017).
- [44] T. Srivastava, W. Lim, I. Joumard, S. Auffret, C. Baraduc, and H. Béa, Mapping different skyrmion phases in double wedges of Ta/FeCoB/TaOx trilayers, *Phys. Rev. B* **100**, 220401(R) (2019).
- [45] S.-Z. Lin, C. Reichhardt, C. D. Batista, and A. Saxena, Particle model for skyrmions in metallic chiral magnets: Dynamics, pinning, and creep, *Phys. Rev. B* **87**, 214419 (2013).
- [46] X. Zhang, G. P. Zhao, H. Fangohr, J. P. Liu, W. X. Xia, J. Xia, and F. J. Morvan, Skyrmion-skyrmion and skyrmion-edge repulsions in skyrmion-based racetrack memory, *Sci. Rep.* **5**, 7643 (2015).
- [47] Y. Hirata, D.-H. Kim, S. K. Kim, D.-K. Lee, S.-H. Oh, D.-Y. Kim, T. Nishimura, T. Okuno, Y. Futakawa, H. Yoshikawa, A. Tsukamoto, Y. Tserkovnyak, Y. Shiota, T. Moriyama, S.-B. Choe, K.-J. Lee, and T. Ono, Vanishing skyrmion hall effect at the angular momentum compensation temperature of a ferrimagnet, *Nat. Nanotechnol.* **14**, 232 (2019).
- [48] S. Zhang, X. Zhang, J. Zhang, A. Ganguly, J. Xia, Y. Wen, Q. Zhang, G. Yu, Z. Hou, W. Wang, Y. Peng, G. Xiao,

- A. Manchon, J. Kosel, Y. Zhou, and X.-X. Zhang, Direct imaging of an inhomogeneous electric current distribution using the trajectory of magnetic half-skyrmions, *Sci. Adv.* **6**, eaay1876 (2020).
- [49] A. Hrabec, J. Sampaio, M. Belmeguenai, I. Gross, R. Weil, S. M. Chérif, A. Stashkevich, V. Jacques, A. Thiaville, and S. Rohart, Current-induced skyrmion generation and dynamics in symmetric bilayers, *Nat. Commun.* **8**, 15765 (2017).
- [50] W. Akhtar, A. Hrabec, S. Chouaieb, A. Haykal, I. Gross, M. Belmeguenai, M. S. Gabor, B. Shields, P. Maletinsky, A. Thiaville, S. Rohart, and V. Jacques, Current-Induced Nucleation and Dynamics of Skyrmions in a Co-Based Heusler Alloy, *Phys. Rev. Appl.* **11**, 034066 (2019).
- [51] S. Woo, K. M. Song, X. Zhang, M. Ezawa, Y. Zhou, X. Liu, M. Weigand, S. Finizio, J. Raabe, M.-C. Park, K.-Y. Lee, J. W. Choi, B.-C. Min, H. C. Koo, and J. Chang, Deterministic creation and deletion of a single magnetic skyrmion observed by direct time-resolved X-ray microscopy, *Nat. Electron.* **1**, 288 (2018).
- [52] See Supplemental Material at <http://link.aps.org/supplemental/10.1103/PhysRevApplied.14.054048> for the magnetic hysteresis data of the sample, measurements to account for Joule heating, and video on the current-driven motion of the magnetic skyrmions.